

Article

A Tunable Optoelectronic Oscillator with Phase-to-Amplitude Modulation Transformation via an Acetylene Reference Cell

Vladimir Lebedev¹, Piotr Agruzov¹ , Igor' Iliyechev¹, Andrei Varlamov¹, Ivan Tatsenko², Andrey Nikitin², Alexey B. Ustinov² , Serguei Stepanov^{3,*} and Alexander Shamray¹ ¹ Department for Quantum Electronics, Ioffe Institute, 194021 St. Petersburg, Russia² Department of Physical Electronics and Technology, St. Petersburg Electrotechnical University, 197022 St. Petersburg, Russia³ Department of Optics, CICESE, Ensenada 22860, BC, Mexico

* Correspondence: steps@cicese.mx

Abstract: Operation modes of the optoelectronic oscillator (OEO), based on a phase electrooptic modulator with an acetylene reference cell as a photonic filter, have been investigated. For the wideband phase-to-amplitude demodulation that was observed when the laser wavelength was tuned to one side of the acetylene absorption line, an additional tunable electronic yttrium iron garnet (YIG) filter was introduced to observe single-mode OEO generation. This configuration generated a stable monochromatic signal in the 4–12 GHz frequency range, with phase noise of -122 dBc/Hz at 10 kHz offset from the carrier frequency. In the narrowband demodulation mode (when one optical modulation sideband was tuned to the acetylene absorption line), the quasi-single-mode oscillation could be observed without additional electronic filtering. In this case, the generation frequency was controlled optically by tuning the laser wavelength.

Keywords: optoelectronic oscillator; phase modulator; self-reference demodulation; acetylene



Citation: Lebedev, V.; Agruzov, P.; Iliyechev, I.; Varlamov, A.; Tatsenko, I.; Nikitin, A.; Ustinov, A.B.; Stepanov, S.; Shamray, A. A Tunable Optoelectronic Oscillator with Phase-to-Amplitude Modulation Transformation via an Acetylene Reference Cell. *Photonics* **2023**, *10*, 196. <https://doi.org/10.3390/photonics10020196>

Received: 22 December 2022

Revised: 27 January 2023

Accepted: 3 February 2023

Published: 12 February 2023



Copyright: © 2023 by the authors. Licensee MDPI, Basel, Switzerland. This article is an open access article distributed under the terms and conditions of the Creative Commons Attribution (CC BY) license (<https://creativecommons.org/licenses/by/4.0/>).

1. Introduction

Optoelectronic oscillators (OEOs) present a new promising class of optoelectronic devices that have attracted the attention of many research groups in recent decades. In the general case, they can be presented by a closed optoelectronic loop [1]. One part of this loop is an optical path that ensures a high coherence length, and the other part is an electronic microwave path that enables high controllability. The proposed applications of the OEOs cover a wide variety of applications requiring high-purity, stable microwave or millimeter wave signals in the form of single monochromatic spectral lines with extremely low phase noise, frequency combs, or signals with more complicated arbitrary waveforms [1,2]. Devices of this type with integrated design are also under development now [3,4].

In the simplest basic configuration of OEO, electrooptic amplitude modulation is used to introduce a microwave signal into the optical path. In turn, direct optical detection by a fast photodiode ensures the transformation of an amplitude-modulated optical signal into the electronic path of the feedback loop. The narrowband electronic or photonic filters [5–7] are utilized to select one particular resonant frequency of the optical path of the loop. To ensure the stability of the OEO generation in this basic configuration, both the operation point of the amplitude modulator and the central frequency of the filter being used are to be locked by additional electronic circuits of the feedback control.

Below we propose an original configuration of the OEO with the phase electrooptic modulator, instead of the generally used amplitude one, and the acetylene reference cell as a phase-to-amplitude demodulator and the photonic filter simultaneously. Unlike the electrooptic amplitude modulator, the phase modulator does not require operation point stabilization and permanently ensures linear response to the modulating microwave signal.

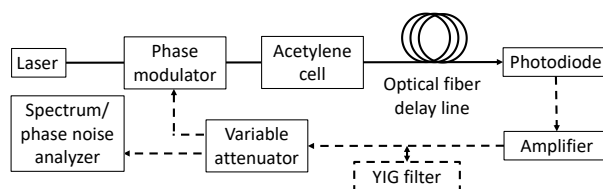
The reference acetylene cell that is used here for demodulation is a highly stable photonic filter in the telecommunication wavelength range (1510–1550 nm) [8]. Indeed, narrow acetylene absorption lines are widely used for laser wavelength locking and stabilization in this highly important spectral range. The low-pressure acetylene reference cells are commercially available and, in particular, in the fiber-coupled configurations. Recently we have demonstrated the utilization of the acetylene cell as a simple and robust optical phase demodulator [9,10] for room temperature operation.

In this paper, we study various demodulation modes, based on the acetylene cell, with respect to OEO operation and, in particular, the possibility of generating a single frequency and tuning it in a broad frequency range. We show that for the broadband demodulation mode, the single mode operation and tunability of the OEO configuration can be ensured by the additional introduction of the electronic YIG spin-wave filter. On the opposite, with narrowband demodulation, the broadband tuning of the generation frequency is reached by optical means only, by tuning the laser wavelength.

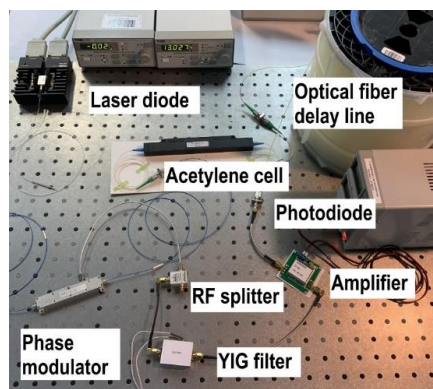
The other important goal of this paper was to investigate an achievable spectral purity and phase noise performance of the proposed OEO configuration. We show, in particular, that the demodulated laser phase noise contributes to the output OEO phase noise. The stability of the generated frequency is, obviously, another important characteristic of the OEO operation. This requires further rather special investigations and is beyond the scope of the present paper.

2. OEO Configuration

A simplified diagram of the proposed OEO is shown in Figure 1a. The photograph of the experimental setup is presented in Figure 1b. In the optical path of the OEO in question, we utilized the “TeraXion” PS-TNL tunable semiconductor laser with low phase noise and with a spectral line width of 1 kHz as a source of the optical carrier. The integrated lithium niobate electrooptic modulator with a frequency bandwidth of 12 GHz at the level of 3 dB and the half-wave voltage $V_{\pi} = 5$ V, fabricated in our group, was utilized for phase modulation of the optical carrier. A single-mode optical fiber (SMF-28) of 2000 m in length was used as an optical delay line. The demodulated output optical signal was detected by a fast photodiode with the frequency bandwidth of about 13 GHz and with the saturation current of 30 mA.



(a)



(b)

Figure 1. (a) A schematic diagram of the OEO under consideration, and (b) a photograph of the experimental setup.

The electronic microwave path of the OEO under consideration also included a low-noise electronic amplifier, a tunable attenuator, a millimeter-wave coupler, and (as an additional frequency-selective element in some experiments) a tunable narrowband (50 MHz) yttrium iron garnet (YIG) spin-wave filter [11–14]. Spectral and noise measurements were performed using the phase noise analyzer Rohde & Schwarz FSWP26.

A commercial “WavelengthReference” bulk acetylene reference cell (with a gas pressure of about 8 Torr) with fiber-optic pigtails was used for demodulation. The most intense acetylene absorption line P9 (with absorbance $\alpha_0 L \approx 2.7$ at the central wavelength of 1530.37 nm [8]) was utilized in the reported experiments. Note that, at room temperature, the low-pressure acetylene demonstrates inhomogeneously broadened (by the Doppler effect) absorption lines of approximately Gaussian shape with a full width at half maximum (FWHM) spectral width of about 500 MHz [9]. The experimentally observed transmittance and absorption spectral curves of the utilized gas cell in the vicinity of the P9 acetylene line are shown in Figure 2.

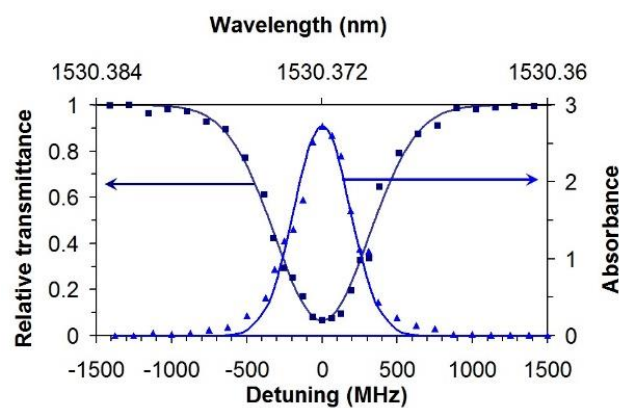


Figure 2. Transmittance/absorbance profiles of the utilized acetylene cell at the P9 spectral line, centered at 1530.372 nm. Solid lines present theoretical fittings with the Gaussian profile of the absorption of 500 MHz FWHM spectral width.

3. Demodulation Modes

The first experiments were carried out with the optical path of the OEO, in an open-loop configuration. Two different modes of phase-to-amplitude modulation conversion (demodulation) with the acetylene reference cell were probed. In the first mode, the broadband one, the demodulation was performed by introducing an additional phase shift to the phase-modulated wave carrier frequency component. To explain this process, let us consider the main difference between the amplitude and the phase sinusoidal modulations.

Equation (1) below represents the amplitude- and phase-modulated signals in the low contrast approximation ($m \ll 1$):

$$\begin{aligned} A_a &= A[1 + m \cdot \cos(\Omega t)]; \\ A_p &= A \cdot \exp[im \cdot \cos(\Omega t)] = A[1 + im \cdot \cos(\Omega t)] \end{aligned} \tag{1}$$

The main difference is, clearly, the $\pi/2$ phase shift between the carrier frequency component and the sidebands. For this reason, to transform an initial phase modulation to the desired amplitude modulation, it is necessary to introduce a similar phase shift between them. If the introduced phase shift is different from $\pm\pi/2$, this transformation (i.e., the demodulation) is, clearly, a partial one only.

In this demodulator configuration, the laser wavelength is tuned to one side of the acetylene absorption line [10], where the phase shift in the transmitted carrier frequency component is maximum; see Figure 3. If the modulation frequency Ω is assumed to be larger than the FWHM spectral width of the line, the output sideband phases are not significantly influenced by the cell.

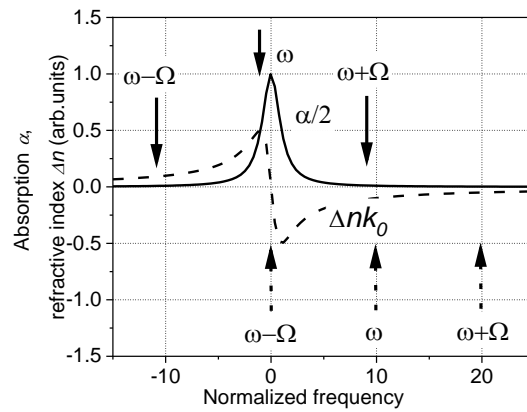
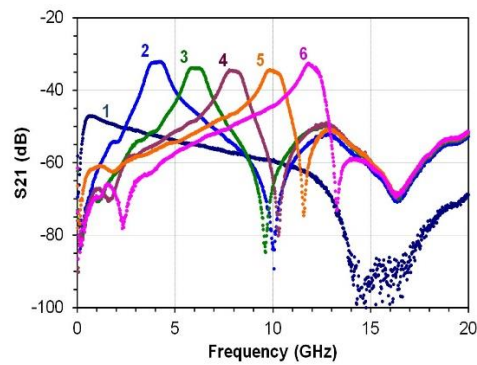
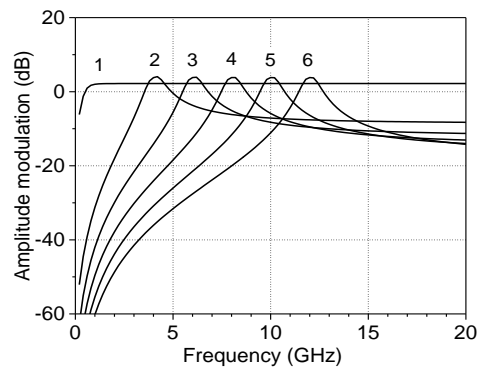


Figure 3. Position of the laser carrier frequency and the modulation sidebands in the acetylene absorption profile (solid line presents the gas amplitude absorption $\alpha/2$, while the dashed line presents the refractive index Δnk_0) for two utilized demodulation modes. Solid arrows correspond to the wideband demodulation and dashed arrows to the narrowband demodulation.

The experimentally observed frequency response of this demodulation mode (i.e., the frequency dependence of the phase-to-amplitude transfer function) is presented in Figure 4a by curve 1. This dependence was obtained in the OEO open-loop configuration with the sinusoidal modulation signal of 0 dBm, applied to the electrooptic phase modulator, and for the incident laser power of 5 mW.



(a)



(b)

Figure 4. (a) Experimentally observed frequency transfer function of the demodulator for the broadband (curve 1) and the narrowband operation modes at different detuning frequencies approximately equal to 0.25 (curve 1), 4 (2), 6 (3), 8 (4), 10 (5), and 12 GHz (6). (b) Theoretical simulations obtained for similar detuning of the laser wavelength from the center of the absorption line with a Lorentzian profile, a maximum absorbance of 3, and an FWHM spectral width of 0.5 GHz.

In the second, the narrowband or selective demodulation mode, the phase-to-amplitude conversion is performed by suppression (and, partially, by change of the phase) of one sideband of the initial phase modulated optical wave. To do this, the laser wavelength is tuned outside of the absorption line, to have one sideband of the modulated signal overlapped with the acetylene absorption/dispersion line (Figure 3).

The experimentally observed frequency dependences of the transfer functions for this demodulation mode are presented in Figure 4a (curves 2–6) for different detuning of the laser wavelength. These dependencies are, clearly, similar to the frequency response of a tunable band-pass filter with the central frequency, corresponding to the laser wavelength detuning from the maximum of the acetylene cell absorption. The FWHM spectral width of this effective filter is determined by the utilized acetylene absorption line.

Note that the frequency responses of the phase modulator, photodetector, and electronic amplifier also contribute to the experimental frequency dependence of the open-loop transfer function. In particular, the cut-off frequency (~13 GHz) in the dependence on the broadband demodulation mode relates to the frequency response of the photodiode with the electronic amplifier, and the slope to the modulator frequency response.

We have performed a theoretical simulation of the demodulation processes. In this analysis, the initial harmonic phase modulation was represented as the sum of a strong carrier frequency component and two weak sidebands shifted up and down by the modulation frequency Ω . The contribution of the higher-order sideband harmonics in phase modulation was neglected in the utilized small-signal approximation [15]. The influence of the acetylene cell was taken into account by multiplying different incident spectral components of the light (the carrier frequency and the two sidebands) by the corresponding amplitude/phase transmittance coefficient of the cell. The absorption line utilized in our simplified simulation was accepted to be of the Lorentzian shape with the complex amplitude transmission coefficient:

$$T = \exp \left\{ \frac{\alpha_0 L}{2} \left[\frac{1}{1 + \left(\frac{\Delta\Omega}{\delta\Omega} \right)^2} + \frac{i \frac{\Delta\Omega}{\delta\Omega}}{1 + \left(\frac{\Delta\Omega}{\delta\Omega} \right)^2} \right] \right\} \quad (2)$$

where $\alpha_0 L$ is the maximum line absorbance, $\Delta\Omega$ is the deviation of the light angular frequency from the center of the absorption line, and $\delta\Omega$ is half of the spectral FWHM width of the line. The intensity modulation amplitude with the Ω modulation frequency was evaluated from the interference of the output optical carrier and sidebands at the quadratic photodetector.

Figure 4b shows the frequency dependences of the output intensity modulation, evaluated for the maximum cell absorbance $\alpha_0 L = 3$, the spectral FWHM line width of 0.5 GHz, and the detuning of the carrier frequency by 0.25, 4, 6, 8, 10, and 12 GHz from the center of the absorption line. One can see a reasonable qualitative agreement with the obtained experimental dependences, presented in Figure 4a.

4. OEO Operation

Now, we go to a discussion of the operation of the closed-loop OEO configuration. Here, first of all, we point to a rather low value of demodulation (about -30 dB), observed even in the maxima of the open-loop transfer functions (Figure 4a), that was due to the low efficiency of electronic–optic–electronic transformation. For this reason, a rather high additional electronic amplification (>30 dB) was required to observe generation in a close-loop configuration of this OEO.

In the OEO with the broadband demodulation, insertion of an additional narrowband pass electronic filter is, obviously, necessary for an acceptable spectral purity generation, i.e., for a low mode-number or a single-frequency operation. Without it, the OEO in question will generate all possible resonance modes of the optical fiber delay line. They are separated by the off-set frequency $\Delta f = c/nL$, where c is the speed of light in vacuum, L is the fiber

length, and n is the effective refractive index of the fiber for the utilized laser wavelength. In the reported experiments with $L \approx 2$ km, Δf is about 0.1 MHz. These generated modes are spread over the total bandwidth of the open-loop arrangement frequency range (~ 13 GHz, see Figure 4a), which is determined by characteristics of the utilized devices: the phase modulator, the photodiode, and the electronic amplifier.

To reduce the number of the generated modes in this demodulation mode, we have additionally inserted a tunable narrowband YIG film spin-wave filter into the electronic path of the loop after the amplifier; see Figure 1a [16,17]. The utilized microwave spin-wave filter was fabricated in our group in the form a YIG film delay line [11,12]. It consists of 5 μm -thick, 2 mm-wide, and 2 cm-long YIG film waveguide and conventional excitation/reception microstrip structures for the spin waves. An important characteristic feature of such a filter is a rather weak dependence of the delay time on the operation frequency. The central frequency can be easily tuned by variation of the bias magnetic field. As a result, the phase noise of the OEOs, based on the YIG film filters, demonstrates relatively weak dependence on the generation frequency [13], in contrast to the resonator-based oscillators. Note that, recently, OEOs with the spin-wave filters are called “magnonic-optoelectronic oscillators” [14].

Typical frequency transfer function of the open-loop configuration with a YIG film spin-wave filter is shown in Figure 5a. The corresponding spectra of the generated signals, experimentally observed for different tuning of the YIG filter, are presented in Figure 5b. A segment of one of these spectra is presented in Figure 5c with higher resolution. It shows that one of the delay line modes is generated mainly, with the suppression of the side modes by ≈ 40 dB. Note that the FWHM spectral width (Figure 5a) of the utilized microwave spin-wave filter ≈ 50 MHz [16] was significantly larger than the intermode spacing of the optical fiber delay line (≈ 0.1 MHz). Such FWHM filter spectral width was sufficient, however, to reach the single-mode generation. Similar single-mode spectra of the generated signals were observed for the entire tuning range (4–12 GHz) of the spin-wave filter. Note that to control the generation frequency in this case, one has to tune the spin-wave filter in the electronic path of the configuration only.

We have also investigated similar OEO operations with the narrowband demodulation via the acetylene cell. In this case, the YIG filter was not utilized, and the acetylene reference cell was used as the only frequency-selective element. This configuration allows us to optically tune the generation frequency by changing the laser wavelength. The range of the frequency tuning in this case is restricted by the frequency bandwidth of the modulator, photodiode, and electronic amplifier.

Typical generation spectra obtained for different tuning of the laser in a broad (0–20 GHz) frequency range are shown in Figure 6a. From one of such spectra, presented in Figure 6b with higher resolution, one can see the mode structure of the oscillations much better. It is clear that the additional, not central, generated modes (side modes) are more intensive than those, observed with the microwave spin-wave filter (Figure 5c). The side modes suppression for the narrowband demodulator operation mode was about 20 dB, while for the 50 MHz YIG filter it was two orders of magnitude better (about 40 dB). It is clear that the spectral width of the acetylene reference cell (500 MHz) is insufficient to ensure a high-purity single-mode OEO operation. One can see that the total spectral width of the generated signal is, however, significantly more narrow than the demodulator bandwidth (Figure 4).

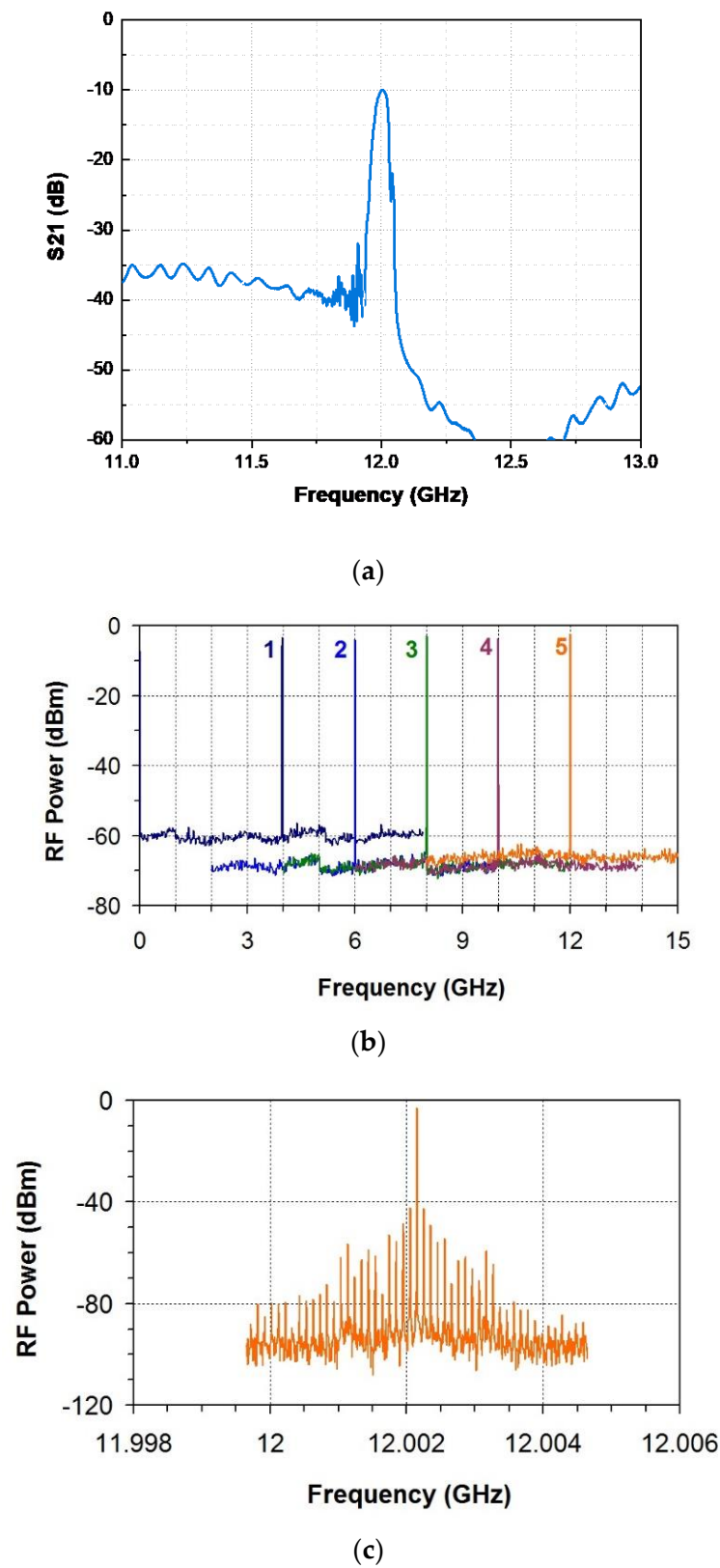


Figure 5. (a) Typical frequency transfer function of the open-loop configuration with the YIG film spin-wave filter, tuned at 12 GHz. (b) Superimposed generation spectra, obtained for OEO configuration with the broadband demodulation for different settings of the YIG filter. (c) Similar generation spectrum observed for tuning of the YIG film filter to ≈ 12 GHz and presented with higher resolution.

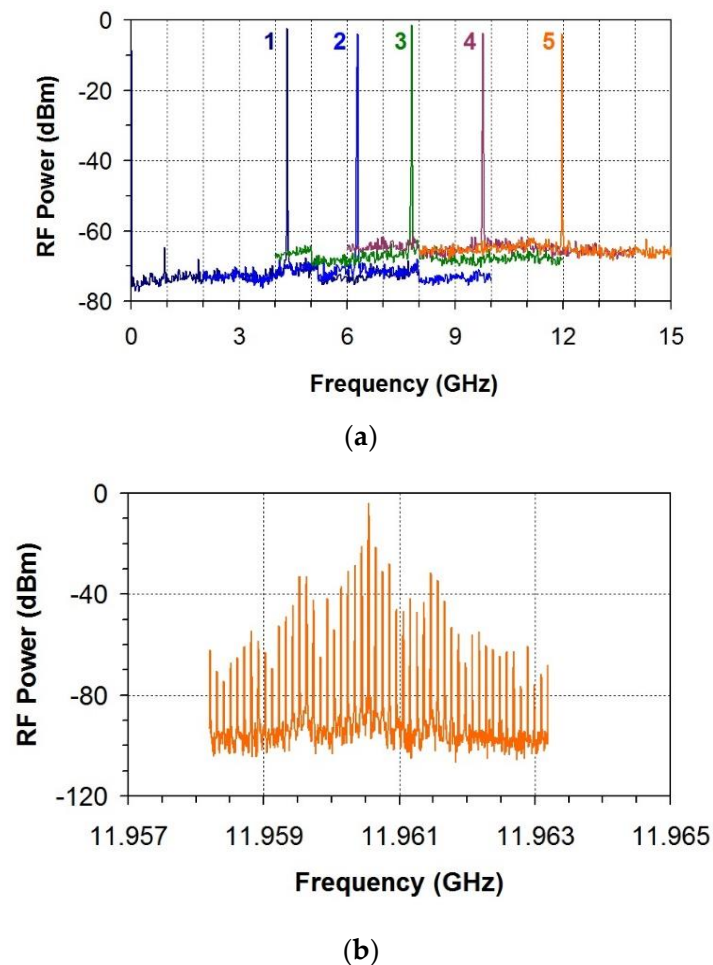


Figure 6. (a) Superimposed generation spectra obtained for the narrowband demodulation mode with different detuning of the carrier wavelength from the acetylene absorption line and (b) the generation spectrum, obtained with 12 GHz detuning and shown with higher resolution.

It was noted above that the spectral selectivity of the narrowband demodulator mode is governed by the inhomogeneous spectral width of the utilized acetylene absorption line. In fact, the homogeneously broadened spectral width of low-pressure acetylene is approximately an order of magnitude smaller [10]. Such narrow spectral transmission lines can be formed by local saturation of the gas optical absorption via the process of a spectral hole burning. Additional, more detailed analysis and investigations are, obviously, needed to understand how such artificially induced narrow transmission peaks can be used for improving the frequency purity of OEOs with the acetylene-based demodulation.

One can expect that simultaneous utilization of the narrowband demodulation mode and the spin-wave YIG filter can further increase the suppression of the side modes. This improvement cannot, however, be very impressive (as compared to that presented in Figure 5c) since the difference in the spectral widths of the YIG filter and the narrowband acetylene-based demodulator is quite large. Additionally, tuning the generation frequency in such a configuration is much more complicated; it, obviously, needs a synchronous change of the laser wavelength and the resonance frequency of the YIG filter.

As was mentioned above, similar spectra of the generated signals were observed at the corresponding tuning of the laser frequency in the whole investigated range (4–12 GHz); see Figure 6a. Note that for small (<10 GHz) detuning of the laser, higher harmonics of the main generation frequency were also observed; see Figure 7. We attribute them to an increased number of the modulation harmonics that appear even for linear phase modulation, as well as to the nonlinearity of the demodulation, photodiode, and electronic amplifier.

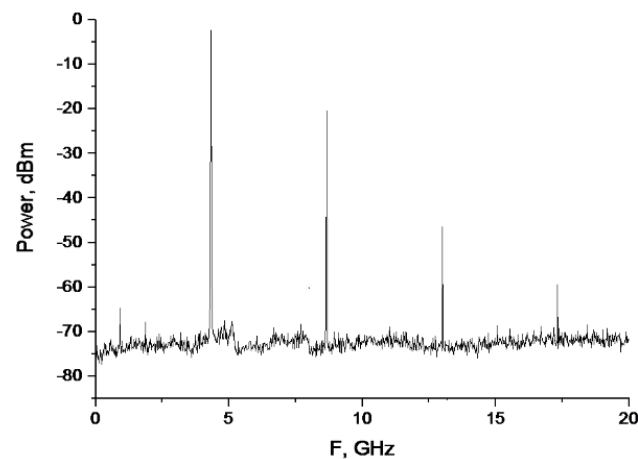


Figure 7. Higher harmonics in the generation spectrum that were observed with the narrowband demodulation without a YIG filter for approximately 4 GHz detuning of the laser frequency from the acetylene absorption line.

5. OEO Noise Characteristics

Figure 8 presents typical dependences of the generated monochromatic signal phase noise as a function of the frequency offset for the broadband demodulation mode with the tunable microwave YIG film filter in the electronic path of the OEO loop. Similar dependences, with the noise floor from -140 dBc/Hz to -130 dBc/Hz, were obtained for all generation frequencies in the range of the YIG film filter tuning (4–12 GHz). The phase noise at the 10 kHz offset was about -122 dBc/Hz. The noise peaks, observed near 100 kHz (i.e., near the intermode distance of the fiber optic delay line), are due to the contribution of the sideband modes. It is the so-called supermode noise, which is inherent to a single-loop OEO configuration.

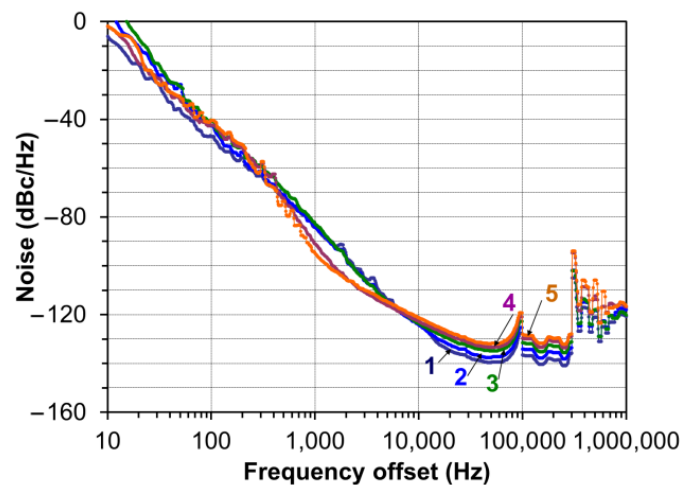


Figure 8. Phase noise in the OEO with the broadband demodulation and tunable YIG filter as a function of the frequency offset at different generation frequencies: curve 1–4, 2–6, 3–8, 4–10, and 5–12 GHz.

The phase noise in the OEO with the narrowband demodulation had similar dependence versus frequency offset (Figure 9). The noise floor was, however, about -132 dBc/Hz for all generation frequencies. A more significant supermode noise contribution is associated with a lower efficiency of the sideband suppression and worse generation frequency purity. Various approaches, such as multiple loops [18], can be utilized for the reduction in these noise peaks and for improving the frequency purity.

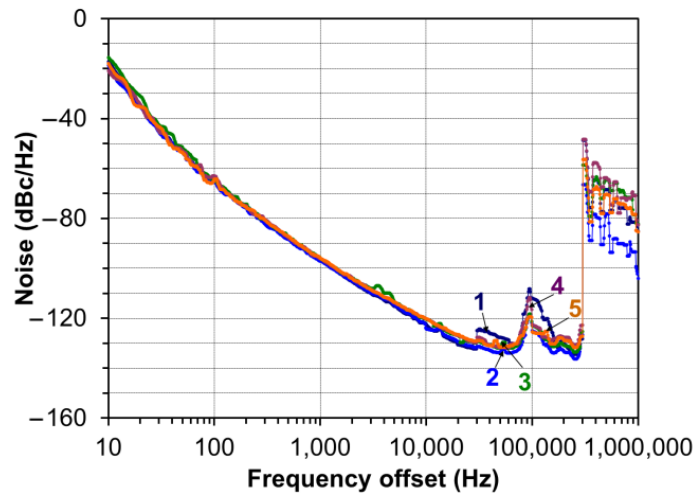


Figure 9. Phase noise in OEO with narrowband demodulation as a function of the frequency offset at different generation frequencies: curve 1–4, 2–6, 3–8, 4–10, and 5–12 GHz.

The theoretical estimation of the oscillator phase noise power spectral density was done using the Yao–Maleki equation [19]:

$$S(f') = \frac{\delta}{\left(2 - \frac{\delta}{\tau}\right) - 2\sqrt{1 - \frac{\delta}{\tau}} \cos(2\pi f'\tau)} \tag{3}$$

where τ is the delay time of the optical fiber line, f' is the frequency offset, and δ is the input noise-to-signal ratio, i.e., the ratio of the input noise power density of the oscillator to the power of oscillations. The model, reported in [19], takes into account the following sources of white noise: the thermal noise of the amplifier, the shot noise of the photodiode, and the effective relative intensity noise (RIN) of the laser. The effective RIN also includes demodulated laser phase noise. It results in an increase in the phase noise with a slope of f^{-2} for the frequency offset smaller than Leeson frequency $f_L = 1/\pi\tau$.

In the OEO under consideration with the optical fiber delay line 2 km long, the value of f_L equals ≈ 32 kHz. Indeed, the experimentally observed phase noise spectrum obtains f^{-2} slope at frequencies lower than this value (Figure 10). For smaller offset frequencies, the experimental phase noise demonstrates the slope f^{-3} from a frequency offset of about 2.8 kHz. One can assume that this is due to the flicker noise (i.e., $1/f$ noise) of the utilized microwave amplifier and the photodetector [20,21].

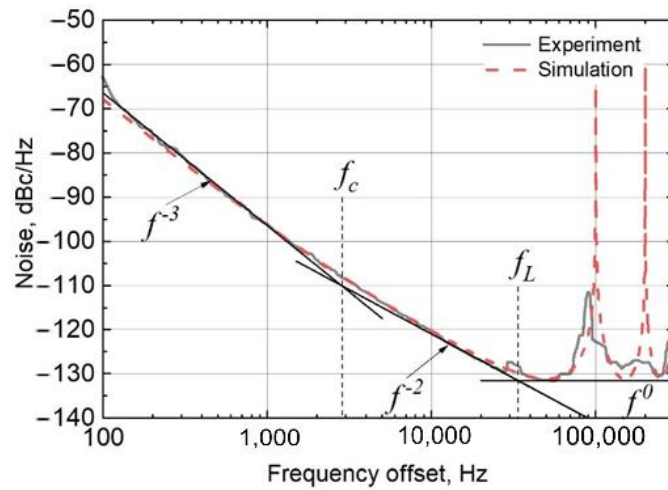
In the standard Yao–Maleki model, the noise-to-signal ratio of white noise can be calculated in the following way:

$$\delta_{white} = \frac{\rho G_A^2}{P_{osc}} \tag{4}$$

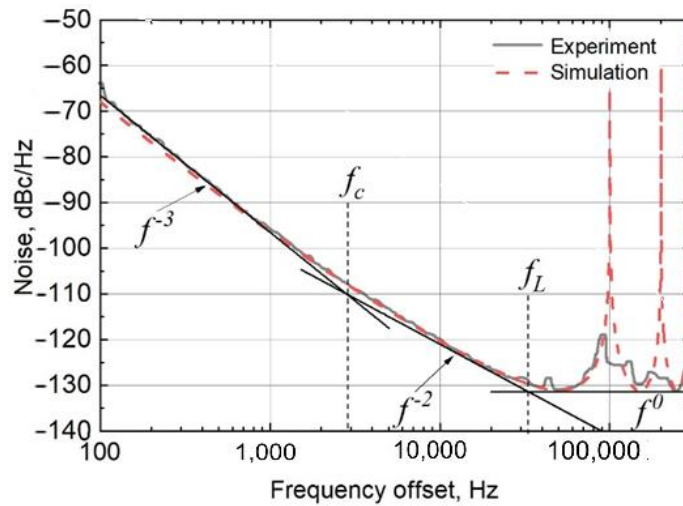
where ρ is the total power density of white noise, G_A is the voltage gain of the microwave amplifier, and P_{osc} is the oscillation power. The presence of flicker noise changes the total noise-to-signal ratio of the OEO generation, as follows:

$$\delta(f) = \delta_{white} + \frac{\delta_{1/f}}{f} \tag{5}$$

Typical results of the numerical simulation are shown by dashed lines in Figure 10. From a comparison of the experimental results and simulations, we found that the noise-to-signal ratio of the $1/f$ noise is $\delta_{1/f} = 5 \cdot 10^{-10}$.



(a)



(b)

Figure 10. Phase noise of the OEO with narrowband demodulation as a function of the frequency offset for a generation frequency of 10 (a) and 12 GHz (b).

It is important to mention that the experimentally observed phase noise floor was approximately 10 dB below that, which was reported earlier for other configurations of OEOs with phase electrooptic modulators [7]. Unlike our experiments, the authors utilized the phase-shifted fiber Bragg grating as a narrowband optical filter. The phase noise floor, reported in [7], was determined by the residual phase noise of the active devices in the OEO loop, such as the thermal noise of the amplifier, the shot noise of the photodiode, and the RIN of the laser. The improvement in the noise performance in our experiments was reached by using a low phase noise laser source and a high saturation current photodiode, capable for the detection of high optical power.

The interested reader can find a more extended comparison of operation characteristics of different earlier investigated configurations of the OEOs in Table 1 of a recent review paper [1].

6. Conclusions

Summarizing, we have presented the results of an experimental study of the original configuration of tunable OEO operating in the 1.5 μm communication wavelength range. Unlike conventional OEOs with amplitude electrooptic modulators, our configuration uses the optical phase modulation and the original demodulation technique, where phase

modulation is transformed into amplitude one via narrow resonance line of a reference acetylene cell.

Two regimes of the OEO operation, corresponding to different demodulation modes with a low-pressure acetylene cell, were studied. The wideband phase-to-amplitude demodulation was ensured by tuning the laser wavelength to one side of the acetylene absorption line. In the narrowband demodulation mode, one of the modulated signal sidebands was tuned to the acetylene absorption line. The microwave spin-wave YIG film filter was used to reach single-frequency operation, to improve generation frequency purity, and to provide electronic tuning in case of the wideband demodulation mode. In the narrowband demodulation mode, additional electronic filtering was not used. The generation frequency was controlled in this case optically by detuning the laser wavelength. Various techniques, such as multiple loops, can be applied to suppress higher sideband modes and improve frequency purity in both investigated OEO configurations.

The improved phase noise characteristics (the phase noise floor of -132 dBc/Hz) have been demonstrated. This noise floor is approximately 10 dB below that reported earlier in a similar OEO with a phase electrooptic modulator and phase-shifted fiber Bragg grating as a narrowband optical filter. The improvement in the noise performance of our OEO configuration was achieved by using a low phase noise laser source and a high-saturation photodiode.

From the point of view of the authors, the most promising areas of practical applications of the proposed OEO configurations are radars and telecommunication systems. A more detailed analysis of all particular requirements (power, frequency range, etc.), is, obviously, needed for a more precise specification.

Author Contributions: Conceptualization, A.B.U., S.S. and A.S.; methodology, V.L., P.A. and A.B.U.; validation, A.B.U., S.S. and A.S.; formal analysis, I.T., A.N., A.V., A.B.U. and S.S.; investigation, V.L., A.V., P.A., I.L., I.T., A.N., A.B.U., S.S. and A.S.; writing—original draft preparation, S.S.; writing—review and editing, A.B.U., S.S. and A.S. All authors have read and agreed to the published version of the manuscript.

Funding: The research in SPbETU was funded by the Ministry of Science and Higher Education of the Russian Federation, grant number FSEE-2020-0005.

Institutional Review Board Statement: Not applicable.

Informed Consent Statement: Not applicable.

Data Availability Statement: The data are available from the first author and the corresponding author upon reasonable request.

Conflicts of Interest: The authors declare no conflict of interest.

References

1. Chembo, Y.K.; Brunner, D.; Jacquot, M.; Larger, L. Optoelectronic oscillators with time-delayed feedback. *Rev. Mod. Phys.* **2019**, *91*, 035006. [[CrossRef](#)]
2. Kondrashov, A.V.; Ustinov, A.B. Self-generation of Möbius solitons and chaotic waveforms in magnonic-optoelectronic oscillators under simultaneous action of optic and magnonic nonlinearities. *J. Appl. Phys.* **2022**, *132*, 173907. [[CrossRef](#)]
3. Tang, J.; Hao, T.; Li, W.; Domenech, D.; Baños, R.; Muñoz, P.; Zhu, N.; Capmany, J.; Li, M. Integrated optoelectronic oscillator. *Opt. Express* **2018**, *26*, 12257. [[CrossRef](#)] [[PubMed](#)]
4. Brunetti, G.; Armenise, M.N.; Ciminelli, C. Chip-Scaled Ka-Band Photonic Linearly Chirped Microwave Waveform Generator. *Front. Phys.* **2022**, *10*, 785650. [[CrossRef](#)]
5. Strelakov, D.; Aveline, D.; Yu, N.; Thompson, R.; Matsko, A.; Maleki, L. Stabilizing an optoelectronic microwave oscillator with photonic filters. *J. Light. Technol.* **2003**, *21*, 3052–3061. [[CrossRef](#)]
6. Xie, X.; Zhang, C.; Sun, T.; Guo, P.; Zhu, X.; Zhu, L.; Hu, W.; Chen, Z. Wideband tunable optoelectronic oscillator based on a phase modulator and a tunable optical filter. *Opt. Lett.* **2013**, *38*, 655–657. [[CrossRef](#)] [[PubMed](#)]
7. Li, W.; Yao, J. A Wideband Frequency Tunable Optoelectronic Oscillator Incorporating a Tunable Microwave Photonic Filter Based on Phase-Modulation to Intensity-Modulation Conversion Using a Phase-Shifted Fiber Bragg Grating. *IEEE Trans. Microw. Theory Tech.* **2012**, *60*, 1735–1742. [[CrossRef](#)]
8. Swann, W.C.; Gilbert, S.L. Pressure-induced shift and broadening of 1510–1540-nm acetylene wavelength calibration lines. *J. Opt. Soc. Am. B* **2000**, *17*, 1263–1270. [[CrossRef](#)]

9. Casillas, N.; Stepanov, S.; Ocegueda, M.; Hernández, E. Utilizing phase memory of a two-level quantum system for adaptive homodyne detection of optical phase modulation. *J. Opt.* **2019**, *21*, 045201. [[CrossRef](#)]
10. Casillas, N.; Stepanov, S.; Ocegueda, M.; Hernández, E. Self-referencing mW-scale detection of sub-ns optical phase modulation in acetylene at 1530 nm. *Appl. Opt.* **2019**, *58*, 6495–6503. [[CrossRef](#)] [[PubMed](#)]
11. Ustinov, A.B.; Drozdovskii, A.V.; Nikitin, A.; Kalinikos, B. Spin-wave band-pass filters based on yttrium iron garnet films for tunable microwave photonic oscillators. *J. Physics: Conf. Ser.* **2015**, *661*, 012058. [[CrossRef](#)]
12. Ustinov, A.B.; Nikitin, A.A.; Kalinikos, B.A. Electronically tunable spin-wave optoelectronic microwave oscillator. *Tech. Phys.* **2015**, *60*, 1392–1396. [[CrossRef](#)]
13. Ustinov, A.B.; Nikitin, A.A.; Kalinikos, B.A. Magnetically Tunable Microwave Spin-Wave Photonic Oscillator. *IEEE Magn. Lett.* **2015**, *6*, 3500704. [[CrossRef](#)]
14. Xiong, Y.; Zhang, Z.; Li, Y.; Hammami, M.; Sklenar, J.; Alahmed, L.; Li, P.; Sebastian, T.; Qu, H.; Hoffmann, A.; et al. Experimental parameters, combined dynamics, and nonlinearity of a magnonic-opto-electronic oscillator (MOEO). *Rev. Sci. Instruments* **2020**, *91*, 125105. [[CrossRef](#)] [[PubMed](#)]
15. Palací, J.; Villanueva, G.; Galán, J.; Martí, J.; Vidal, B. Single bandpass photonic microwave filter based on a notch ring resonator. *IEEE Photonics Technol. Lett.* **2010**, *22*, 1276–1278. [[CrossRef](#)]
16. Ustinov, A.B.; Nikitin, A.; Lebedev, V.V.; Serebrennikov, A.; Shamray, A.V.; Kondrashov, A.V.; Kalinikos, B. A Low Phase Noise Tunable Microwave Spin Wave Optoelectronic Oscillator. *J. Physics Conf. Ser.* **2018**, *1038*, 012033. [[CrossRef](#)]
17. Ustinov, A.B.; Kondrashov, A.V.; Nikitin, A.; Lebedev, V.V.; Petrov, A.N.; Shamrai, A.; Kalinikos, B. A tunable spin wave photonic generator with improved phase noise characteristics. *J. Physics: Conf. Ser.* **2019**, *1326*, 012015. [[CrossRef](#)]
18. Yao, X.S.; Maleki, L. Multi-loop optoelectronic oscillator. *IEEE J. Quant. Electron.* **2000**, *36*, 79. [[CrossRef](#)]
19. Yao, X.S.; Maleki, L. Optoelectronic microwave oscillator. *J. Opt. Soc. Am. B* **1996**, *13*, 1725–1735. [[CrossRef](#)]
20. Rubiola, E.; Salik, E.; Yu, N.; Maleki, L. Flicker noise in high-speed pin photodiodes. *IEEE Trans. Microw. Theory Tech.* **2006**, *54*, 816–820. [[CrossRef](#)]
21. Rubiola, E. *Phase Noise and Frequency Stability in Oscillators*; Cambridge University Press: Cambridge, UK, 2008; 228p.

Disclaimer/Publisher's Note: The statements, opinions and data contained in all publications are solely those of the individual author(s) and contributor(s) and not of MDPI and/or the editor(s). MDPI and/or the editor(s) disclaim responsibility for any injury to people or property resulting from any ideas, methods, instructions or products referred to in the content.